HHS Public Access

Author manuscript

Cell Metab. Author manuscript; available in PMC 2016 May 05.

Published in final edited form as:

Cell Metab. 2015 May 5; 21(5): 692–705. doi:10.1016/j.cmet.2015.04.008.

Central serotonergic neurons activate and recruit thermogenic brown and beige fat and regulate glucose and lipid homeostasis

Jacob M. McGlashon[1,4,5], **Michelle C. Gorecki**[1,4,5], **Amanda E. Kozlowski**[1], **Caitlin K. Thirnbeck**[1], **Kathleen R. Markan**[2], **Kirstie L. Leslie**[1], **Maya E. Kotas**[3], **Matthew J. Potthoff**[2], **George B. Richerson**[1], and **Matthew P. Gillum**[1,4,5]

[1]Department of Neurology, University of Iowa Carver College of Medicine, Iowa City, IA, 52242, USA

[2]Department of Pharmacology, University of Iowa Carver College of Medicine, Iowa City, IA, 52242, USA

[3]Department of Medicine, Columbia University College of Physicians and Surgeons, New York, NY, 10032, USA

[4]Novo Nordisk Foundation Center for Basic Metabolic Research, University of Copenhagen, 2200 Copenhagen, Denmark

[5]Institute of Biomedical Sciences, University of Copenhagen, 2200 Copenhagen, Denmark

Summary

Thermogenic brown and beige adipocytes convert chemical energy to heat by metabolizing glucose and lipids. Serotonin (5-HT) neurons in the central nervous system are essential for thermoregulation and accordingly may control metabolic activity of thermogenic fat. To test this, we generated mice in which the human diphtheria toxin receptor was selectively expressed in central 5-HT neurons. Treatment with diphtheria toxin eliminated 5-HT neurons and caused loss of thermoregulation, brown adipose tissue (BAT) steatosis, and a >50% decrease in uncoupling protein 1 (*Ucp1*) expression in BAT and inguinal white adipose tissue (WAT). In parallel, blood glucose increased 3.5-fold, free fatty acids 13.4-fold and triglycerides 6.5-fold. Similar BAT and beige fat defects occurred in *Lmx1b*$^{f/f/p}$ mice, in which 5-HT neurons fail to develop *in utero*. We conclude 5-HT neurons play a major role in regulating glucose and lipid homeostasis, in part through recruitment and metabolic activation of brown and beige adipocytes.

Introduction

Brown fat is a specialized thermogenic organ in mammals that produces heat by uncoupling substrate oxidation from electron transport using the mitochondrial proton channel uncoupling protein 1. In performing this function, BAT consumes up to one hundred times

Contact information:gillum@sund.ku.dk, +45 23 64 89 95.

Author Contributions

Performed research and analyzed data: J.M.M.; A.E.K.; M.C.G.; C.K.T.; K.R.M.; M.E.K.; M.J.P.; G.B.R.; M.P.G. Wrote manuscript: M.P.G.; G.B.R.; J.M.M.

more energy per gram than any other tissue (Cannon and Nedergaard, 2004). Thus, even in small quantities, activated BAT can be a major contributor to whole-body energy metabolism. In rodents housed below thermoneutral ambient temperatures, BAT can burn up to 50% of ingested triglycerides and 75% of ingested glucose (Nedergaard et al., 2011). As a result, cold-induced, BAT-mediated clearance of triglyceride-rich lipoproteins is curative in murine models of hyperlipidemia and glucose intolerance (Bartelt et al., 2011). Interestingly, *Ucp1*-expressing cells have also been observed in subcutaneous WAT (scWAT) depots, which were not previously thought to participate in energy expenditure. Such adipocytes, often referred to as "beige" or "brite," also contribute to thermoregulation and resistance to metabolic disease (Cohen et al., 2014; Jespersen et al., 2013; Shabalina et al., 2013; Wu et al., 2013). Recruitment of "beige" cells is referred to as "browning". Both brown and beige adipocytes are present in adult humans, albeit in lesser quantities relative to body weight than in rodents, and pharmacological stimulants of their activity are being sought as treatments for obesity, type 2 diabetes, and dyslipidemia (Cohade et al., 2003; Cypess et al., 2009; Huttunen et al., 1981; van Marken Lichtenbelt et al., 2009; Nedergaard et al., 2007; Tanuma et al., 1976; Virtanen et al., 2009; Yoneshiro et al., 2013). Discovering such molecules remains the defining challenge in the field (Cypess et al., 2012; Kajimura and Saito, 2014).

In both rodents and humans, the sympathetic nervous system regulates BAT mass and activity. Both activation and expansion of BAT require that norepinephrine (NE) be released from postganglionic sympathetic nerve terminals to stimulate lipid oxidation through the β_3-adrenoreceptor (Beviz et al., 1968; Hsieh and Carlson, 1957; Zhao et al., 1994). In mice, genetic deletion of the NE-synthesizing enzyme dopamine β-hydroxylase leads to accumulation of lipid in BAT, a decrease in expression of *Ucp1*, and cold intolerance (Thomas and Palmiter, 1997). In humans, NE secretion by tumors leads to an increase in abundance and activity of BAT (English et al., 1973), while administration of the β-adrenergic receptor antagonist propranolol blocks BAT activation during cold exposure (Söderlund et al., 2007). NE also appears to be important for recruitment of beige fat (Harms and Seale, 2013). However, NE has many other effects in both the central and peripheral nervous systems, affecting cognition, blood pressure, cardiac output, and visceral-organ function. Thus, to be therapeutically useful, stimulation of NE release would have to be limited to only brown and beige fat.

In humans, mild cold exposure stimulates brown fat metabolism and peripheral vasoconstriction without influencing sympathetic activity in other tissues (Cypess et al., 2012). This selectivity is mediated by specialized sympathetic premotor neurons in the brainstem (Cano et al., 2003; Smith et al., 1998; Strack et al., 1989). Specifically, neurons of the rostral raphé pallidus (rRPa) increase thermogenesis and vascular tone, while other sympathetic premotor neurons nearby control different physiological processes (Morrison, 1999). The thermoregulatory rRPa sympathetic premotor neurons integrate signals from peripheral thermoreceptors, the hypothalamus, and other parts of the brain involved in processing temperature-related stimuli in order to stimulate sympathetic output that activates BAT (Morrison et al., 2014; Nakamura and Morrison, 2011). Thus, they represent a convergence point in a distributed neural network that controls BAT activation. Therefore,

one potential strategy for selectively triggering NE release in BAT would be to activate these sympathetic premotor neurons. However, their molecular identity remains incompletely characterized. Moreover, which rRPa neurons activate and recruit beige fat—if any—remains unknown.

Within the rRPa there are neurons that contain 5-HT, others that express *vGlut3*, and some that contain both 5-HT and *vGlut3* (Nakamura et al., 2004). Previous work has focused on *vGlut3*-expressing sympathetic premotor neurons in the rRPa in activating BAT (Morrison et al., 2014; Nakamura and Morrison, 2011; Nakamura et al., 2004). However, several studies have also suggested that central 5-HT neurons participate in BAT activation. For example, neuroanatomical tract tracing experiments show that *Tph2*+ serotonergic neurons are part of the circuit that connects the brain to BAT (Cano et al., 2003). Retrograde viral tracing studies of sympathetic nerves terminating in scWAT labels cells in the IML of the spinal cord and the raphé pallidus (Nguyen et al., 2014). Interestingly, the IML is densely innervated by 5-HT neurons, many of whose cell bodies reside in the raphé pallidus (Loewy, 1981). Other *in vivo* studies show that 5-HT neurons of the rRPa increase their firing rate in response to cold (Nason and Mason, 2006) and that targeting 5-HT receptors pharmacologically in the raphé or spinal cord affects cold-evoked sympathetic nerve activity in brown fat (Madden and Morrison, 2006, 2010; Nakamura and Morrison, 2011). In addition, central administration of *para*-chlorophenylalanine (PCPA), an inhibitor of 5-HT biosynthesis, inhibits BAT thermogenesis and causes BAT steatosis (Fuller et al., 1987). Further, studies in genetically engineered animals demonstrate an indispensable role for 5-HT neurons in thermogenesis—but not thermosensation or heat conservation—at normal room temperature (Ray et al., 2011), or when exposed to an ambient temperature of 4°C (Hodges et al., 2008, 2011). Most recently, it was demonstrated that lesioning central 5-HT neurons in adult animals with DT causes hypothermia. However, the mechanism was not identified in that study (Cerpa et al., 2014). Finally, it is notable that a human syndrome of inappropriate serotonergic excess—serotonin syndrome—is characterized by hyperthermia. Although a major component of hyperthermia in serotonin syndrome is due to heat generation by muscle contraction and can be reversed by treatment with paralytic agents (Boyer and Shannon, 2005), it cannot be ruled out that the increase in sympathetic output that also occurs may contribute to heat generation by inappropriate activation of BAT.

We hypothesized that central 5-HT signaling would be essential for sympathetic induction of *Ucp1* expression and activity in BAT. Moreover, since sympathetic stimulation of BAT and beige fat occurs simultaneously *in vivo* under physiological conditions (e.g. in response to cold), we hypothesized that the central 5-HT system would also effect the conversion of white adipocytes to active beige adipocytes, as well as the recruitment of new beige fat cells from progenitor populations.

Results

Ablation of Pet-1+ 5-HT neurons inhibits thermogenesis by interscapular BAT

To investigate the role of 5-HT neurons in controlling BAT and beige fat activity, we employed a model of inducible 5-HT neuron ablation, the $DTR^{f/f}ePet1^{Cre}$ mouse, which expresses the human diphtheria toxin receptor (DTR) in CNS 5-HT neurons (Buch et al.,

2005). In this model, systemic injection of diphtheria toxin (DT) eliminates 80% of *Pet-1+* 5-HT neurons in the medulla, including the raphé pallidus (Cerpa et al., 2014), yielding a decrease in core body temperature (T_{core}) from 37 °C to 30–35°C at an ambient temperature of 22°C (Cerpa et al., 2014). Baseline BAT temperature (T_{BAT}) measured with interscapular telemetry temperature probes did not differ between $DTR^{f/f}ePet1^{Cre}$ mice (37.9±0.3°C, n=7) and littermate controls (38.1±0.1°C, n=6). However, three days after mice received intraperitoneal DT injections, T_{BAT} was 1.6°C lower in $DTR^{f/f}ePet1^{Cre}$ mice (36.8 ± 0.3°C, n=7 vs 38.4 ± 0.2°C, n=6; P<0.003). By day four after injection, T_{BAT} in these animals had fallen by 4.0°C (34.0 ± 0.9°C, n=7 vs 38.0 ± 0.3°C, n=6; P<0.003) (Figure 1A).

To exclude the possibility that ablation of 5-HT neurons caused anapyrexia, where a lower T_{core} is actively defended by the CNS, we studied DT-treated $DTR^{f/f}ePet1^{Cre}$ and control mice at a thermoneutral ambient temperature (30°C) (Nedergaard and Cannon, 2014). Even at thermoneutrality, mice can reduce their T_{core} by increasing heat loss or through behavioral mechanisms. Thus, mice exhibit 2°C circadian oscillations in T_{core} when housed at thermoneutrality (Gerhart-Hines et al., 2013). Therefore, T_{core} of anapyrexic animals should still differ from controls. However, under thermoneutral conditions, T_{core} of DT-treated $DTR^{f/f}ePet1_{Cre}$ mice was identical to that of wild-type mice (36.9 ± 0.4°C, n=4 in controls vs. 36.5 ± 0.2°C, n=4 in DT-treated $DTR^{f/f}ePet1^{Cre}$ mice, P=0.34), suggesting that their hypothermia at 22°C resulted from an inability to engage thermogenesis, rather than anapyrexia.

Ablation of Pet-1+ 5-HT neurons causes steatosis in interscapular BAT

Brown adipocytes have a distinctive morphology characterized by the presence of many small intracellular lipid droplets. These droplets shrink as BAT activity increases and expand as it decreases (Cameron and Smith, 1964), inversely tracking with oxidative activity of the tissue. For example, BAT from $Ucp1^{-/-}$ mice, which cannot uncouple mitochondrial respiration, contains large lipid droplets (Enerbäck et al., 1997). H&E staining (Figure 1B–G) of BAT from $DTR^{f/f}ePet1^{Cre}$ mice four days after DT treatment revealed tissue that was steatotic compared to controls. High magnification revealed large, often unilocular lipid droplets, reminiscent of BAT from mice in which *Ucp1* is deleted—and sometimes even of WAT (Enerbäck et al., 1997). Analysis of lipid droplet number and area (Figure 1H and I) in these sections demonstrated a 59% reduction in total number of lipid droplets per imaging field in DT-treated $DTR^{f/f}ePet1^{Cre}$ mice (10,722 ± 854.2 per field, n=9 in control vs. 4,401 ± 1,058 per field, n=3 in DT-treated $DTR^{f/f}ePet1^{Cre}$ mice; P<0.003), which was attributable to a decrease in abundance of very small (<130 μM^2) lipid droplets, which normally represent 60–90% of the total in wild type mice housed at subthermoneutral temperatures. This decrease in abundance of very small droplets was accompanied by a 2.6-fold increase in large lipid droplets >260μM^2 (314 ± 76 per field, n=9 in controls vs. 830 ± 44, n=3 in DT-treated $DTR^{f/f}ePet1^{Cre}$ mice; P<0.004) and a 20-fold increase in lipid droplets >620μM^2 (8 ± 3 per field, n=9 in controls vs. 164 ± 95, n=3; P<0.01), suggesting that pre-existing small lipid droplets expanded and fused to form larger droplets in DT-treated $DTR^{f/f}ePet1^{Cre}$ animals. Together, these data suggest that metabolic activity of interscapular BAT is reduced after loss of *Pet-1+* CNS neurons, leading fatty acids to accumulate—and lipid droplets to expand—within brown adipocytes.

CNS-directed NE release from postganglionic sympathetic nerves triggers intracellular lipolysis, which is required for fat oxidation and lipid droplet breakdown. We hypothesized that emergence of large lipid droplets might be due to impaired sympathetic stimulation of BAT in DT-treated *DTR$^{f/f}$ePet1^{Cre}* mice in response to cold. Supporting this view, at thermoneutrality (30°C), when sympathetic nerve activity is minimized, we found that there was no difference between controls and DT-treated *DTR$^{f/f}$ePet1^{Cre}* mice in average BAT lipid droplet area (87.1 ± 6.6 μM^2, n=5 in controls vs. 79.2 ± 4.0 μM^2, n=4 in DT-treated *DTR$^{f/f}$ePet1^{Cre}* mice; P=0.37), droplet number per 40× field (1,561 ± 108 droplets, n=5 in control vs. 1,653 ± 96 droplets, n=4 in DT-treated *DTR$^{f/f}$ePet1^{Cre}* mice; P=0.54), or droplet size distribution (Figure 2C–E). In contrast, average BAT lipid droplet area in DT-treated *DTR$^{f/f}$ePet1^{Cre}* was increased 3-fold at 22°C (155.7 ± 54.2 μM^2, n=3 in DT-treated *DTR$^{f/f}$ePet1^{Cre}* mice vs. 52.7 ± 4.7 μM^2, n=9 in controls; P<0.006). Thus, whereas lipid droplet area in controls decreased by 45% between 30°C and 22°C, lipid droplet size in DT-treated *DTR$^{f/f}$ePet1^{Cre}* BAT tended to increase (Δ=+76.5 ± 54.2 μM^2 in droplet area in DT-treated *DTR$^{f/f}$ePet1^{Cre}* mice, n=3 vs Δ=−34.4 ± 14.0 μM^2 in droplet area in control mice, n=9; P<0.0091) (Figure 2A–B, F). These data suggest that sympathetic activation of BAT during mild cold exposure (22°C) is impaired in mice lacking central 5-HT neurons.

Ablation of Pet-1+ 5-HT neurons causes hyperglycemia and hyperlipidemia via BAT-dependent and BAT-independent mechanisms

In other models, an increase in activity and mass of BAT leads to improved glucose and lipid homeostasis (Bartelt et al., 2011; Nedergaard et al., 2011). Therefore, we hypothesized that DT-treated *DTR$^{f/f}$ePet1^{Cre}* mice, which have hypoactive BAT, might exhibit dysregulated glucose and lipid metabolism. We measured glucose, fatty acids, and triglycerides in plasma of DT-treated *DTR$^{f/f}$ePet1^{Cre}* and control mice. *Ad libitum* fed DT-treated *DTR$^{f/f}$ePet1^{Cre}* mice became hyperglycemic and hyperlipidemic, exhibiting a 3.5-fold increase in blood glucose (537 ± 16 mg/dL, n=6 vs 150 ± 9 mg/dL, n=4; P<0.003), a 13.4-fold increase in plasma free fatty acids (0.738 ± 0.090 mM, n=6 vs 0.055 ± 0.023 mM, n=3; P<0.024), and a 6.5-fold increase in plasma triglycerides (188 ± 50 mg/dL, n=6 vs 29 ± 4 mg/dL, n=4; P<0.02) (Figure 3A–C).

Since increases in glucose and fatty acid levels of comparable magnitude are seen with insulin deficiency, we measured circulating levels of insulin and hormones that regulate insulin secretion. After intraperitoneal (i.p.) DT treatment, insulin levels decreased by 83% in *DTR$^{f/f}$ePet1^{Cre}* mice (0.24 ± 0.02 ng/ml, n=4 in controls vs 0.04 ± 0.014 ng/ml in DT-treated *DTR$^{f/f}$ePet1^{Cre}*, n=4; P<0.0002). This was accompanied by a 2.2 fold increase in corticosterone (234 ± 60 ng/ml, n=4 in controls vs 504.6 ± 66 ng/ml in DT-treated *DTR$^{f/f}$ePet1^{Cre}* mice, n=6; P<0.022) and a 56% drop in thyroid stimulating hormone (TSH) in DT-treated *DTR$^{f/f}$ePet1^{Cre}* mice (886 ± 159 pg/ml, n=4 in controls vs 393 ± 125 pg/ml in DT-treated *DTR$^{f/f}$ePet1^{Cre}*, n=6; P<0.039) (Figure 3D–F). Circulating epinepherine and NE levels did not differ between groups (data not shown).

These data led to the hypothesis that an inability to oxidize fatty acids and glucose in BAT —possibly combined with cold stress—might be responsible for the steady-state increases in circulating fatty acids, glucose, and triglycerides in DT-treated *DTR$^{f/f}$ePet1^{Cre}* mice. This is

likely due to reduced substrate disposal in BAT, as well as by corticosterone-mediated suppression of insulin secretion (which would promote lipolysis and increased hepatic glucose production). To test this, we measured these metabolites in control and DT-treated *DTR*$^{f/f}$*ePet1*^{Cre} mice housed at thermoneutrality (30°C), anticipating that this change in ambient temperature would eliminate BAT-dependent differences in plasma metabolites. Housing at 30°C abolished significant intergroup differences in corticosterone (396.1 ± 66.17 ng/ml, n=5 in controls vs 478.7 ± 67.74 ng/ml in DT-treated *DTR*$^{f/f}$*ePet1*^{Cre} mice, n=4; P=0.417) and insulin levels (0.0874 ± 0.01685 ng/ml, n=5 in controls vs 0.03675 ± 0.01377 ng/ml in DT-treated *DTR*$^{f/f}$*ePet1*^{Cre} mice, n=4; P=0.060) (though insulin still trended lower), suggesting that cold-induced corticosterone production might inhibit insulin secretion in DT-treated *DTR*$^{f/f}$*ePet1*^{Cre} mice housed at 22°C (Figure 3G and H). While plasma triglycerides remained increased at 30°C in DT-treated *DTR*$^{f/f}$*ePet1*^{Cre} mice (35.21 ± 2.108 mg/dL, n=5 in controls vs 74.79 ± 12.79 mg/dL in DT-treated *DTR*$^{f/f}$*ePet1*^{Cre} mice, n=4; P<0.05), the magnitude of this change was less than at 22°C (2.1-fold vs. 6.5-fold) (Figure 3I). Similarly, plasma fatty acid levels were significantly increased at 30°C (0.373 ± 0.036 mM, n=5 in controls vs 0.753 ± 0.084 mM in DT-treated *DTR*$^{f/f}$*ePet1*^{Cre} mice, n=4; P<0.01), but to a lesser extent than at 22°C (2-fold vs. 13.4-fold) (Figure 3J). On the other hand, glucose levels in DT-treated *DTR*$^{f/f}$*ePet1*^{Cre} mice remained elevated at thermoneutrality (180.6 ± 7.1 mg/dL, n=5 in controls vs 536.5 ± 22.0 mg/dL in DT-treated *DTR*$^{f/f}$*ePet1*^{Cre} mice, n=4; P<0.0001), to an extent similar to 22°C (3-fold vs. 3.5-fold) (Figure 3K). These results suggest that minimizing BAT activity in both control and DT-treated *DTR*$^{f/f}$*ePet1*^{Cre} mice reduces the difference between groups in circulating triglyceride and fatty acid levels. This is consistent with the interpretation that changes in BAT activity may be responsible, in part, for differences in steady-state lipid (but not glucose) levels between control and DT-treated *DTR*$^{f/f}$*ePet1*^{Cre} mice.

The cell type-specificity of *ePet1*-Cre has been validated using Cre-dependent reporter strains, and is highly-specific for CNS 5-HT neurons. However, small numbers of cells in gut, pancreas, skin, and cardiac neural crest also express *ePet1*-Cre during development and/or adult life (Ohta et al., 2011; Scott et al., 2005). Accordingly, these cells may express human DTR and be lesioned by systemic DT treatment in *DTR*$^{f/f}$*ePet1*^{Cre} mice. Thus, we investigated *ePet1*-Cre mediated DTR expression in various tissues by quantitative polymerase chain reaction (qPCR), hypothesizing that lesioning *ePet1*-Cre+ cells in peripheral tissues (in particular pancreatic β-cells) might contribute to hyperglycemia. However, *Hbegf* (the DTR receptor) mRNA was very low in *DTR*$^{f/f}$*ePet1*^{Cre} mouse pancreas, BAT, and liver, consistent with the low levels of adult expression of *Pet-1* in these tissues. By contrast, expression of *Hbegf* mRNA was 1,213-fold higher in raphé, and 314-fold higher in spinal cord than in pancreas, mirroring the adult expression pattern of *Pet-1* (Supplementary Figure 1A and B).

To determine whether *Pet-1*+ cells in the CNS were the critical determinants of the thermogenic and metabolic phenotype seen in *DTR*$^{f/f}$*ePet1*^{Cre} mice treated systemically with DT, we injected DT or vehicle into the lateral ventricle of *DTR*$^{f/f}$*ePet1*^{Cre} mice, and measured BAT temperature and blood glucose daily. This intracerebroventricular (i.c.v.) administration of DT spares DTR+ β-cells of mice that express DTR in both pancreas and

brain under control of RIP-Cre (Rother et al., 2012). Remarkably, four days after treatment, BAT temperature decreased by 7.8°C in i.c.v. DT-treated *DTR*$^{f/f}$*ePet1*^{Cre} mice but remained stable in controls (37.1 ± 0.3°C, n=4 in controls vs. 29.3 ± 2.3°C, n=3 in DT-treated *DTR*$^{f/f}$*ePet1*^{Cre} mice; P<0.01) (Figure 4A). As in systemically DT-treated *DTR*$^{f/f}$*ePet1*^{Cre} mice, this fall in BAT temperature was associated with a 4.2 fold increase in blood glucose levels (165 ± 11 mg/dL, n=4 in controls vs. 689 ± 23 mg/dL, n=3 in i.c.v. DT-treated *DTR*$^{f/f}$*ePet1*^{Cre} animals; P<0.0001) (Figure 4B). Substantially smaller doses of DT were required when administered i.c.v. in order to obtain this effect (75 ng i.c.v. vs. 2.25 μg i.p.). These results indicate that the *Pet-1+* neurons responsible for controlling thermogenesis and systemic glycemia/lipemia reside within the CNS.

Notably, at day four, insulin levels in i.c.v DT-treated *DTR*$^{f/f}$*ePet1*^{Cre} mice did not differ from controls, despite their hyperglycemia (Figure 4C). Thus, we hypothesized that the hyperglycemia caused by deletion of *Pet-1+* neurons was due to elevated rates of endogenous glucose production. To test this possibility, we measured expression of gluconeogenic genes in the liver by qPCR. Consistent with this hypothesis, expression of phosphoenolpyruvate carboxykinase (PEPCK) was elevated 2-fold (2.0 ± 0.38 in i.c.v. DT-treated *DTR*$^{f/f}$*ePet1*^{Cre} mice, n=4 vs 1.0 ± 0.03 in controls, n=4; P<0.042) and glucose-6-phosphatase (G6Pase) was elevated 3.4-fold (4.2 ± 0.77 in i.c.v. DT-treated *DTR*$^{f/f}$*ePet1*^{Cre} mice, n=4 vs 1.2 ± 0.41 in controls, n=4; P<0.014) (Figure 4D and E). This observation may be explained by altered CNS output to liver, but could also involve changes in insulin sensitivity.

Ablation of Pet-1+ 5-HT neurons reduces expression of norepinepherine-responsive thermogenic genes in BAT

Ucp1 and deiodinase 2 (*Dio2*) are prototypical genes expressed by BAT, and increase in response to sympathetic stimulation by NE. Altered expression of these genes would further suggest differential noradrenergic activity in BAT. We found that BAT expression of *Ucp1* mRNA was reduced by 50% in DT-treated *DTR*$^{f/f}$*ePet1*^{Cre} mice compared to controls (0.50 ± 0.13 fold, n=6 vs 1.02 ± 0.09 fold, n=6 in controls; P<0.0085) and expression of *Dio2* was reduced by 85% (0.15 ± 0.06 fold, n=6 vs 1.00 ± 0.2 fold, n=6 in controls; P<0.006) (Figure 5A and B). Notably, markers of BAT differentiation, *Cidea* and *Prdm16*, did not differ between DT-treated *DTR*$^{f/f}$*ePet1*^{Cre} and control mice (*Prdm16*=0.97 ± 0.1 fold, n=5 vs 1.03 ± 0.12 fold, n=6 in controls; P=0.7) and (*Cidea*=0.83 ± 0.14 fold, n=5 vs 1.01 ± 0.07 fold, n=6 in controls; P=0.25), suggesting that the differentiation state of interscapular brown adipocytes was not affected by the ablation of *Pet-1+* neurons. These findings suggest that the low T_{BAT} and extensive lipid vacuolization observed in DT-treated *DTR*$^{f/f}$*ePet1*^{Cre} mice were due to a decrease in release of NE from sympathetic nerves, since at 22°C this is the primary mechanism that drives BAT substrate oxidation, and is continuously activated (Cannon and Nedergaard, 2004; Nedergaard and Cannon, 2014).

In mice treated with i.c.v. DT, similar results were obtained, with BAT expression of *Ucp1* mRNA reduced by 73% (0.29 ± 0.1 fold in i.c.v. DT-treated *DTR*$^{f/f}$*ePet1*^{Cre} mice, n=4 vs 1.07 ± 0.24 fold in controls, n=4; P<0.023) (Figure 5C). Cumulatively, these data support

the hypothesis that central 5-HT neurons modulate the activity—but not the development or differentiation—of BAT cells.

Ablation of Pet-1+ 5-HT neurons reduces expression of thermogenic genes in beige adipose tissue

Recently it has become clear that beige adipocytes can have important effects on metabolic homeostasis and thermoregulation. In general, activation of brown and beige fat appear to be responsive to the same signals and are temporally synchronized, suggesting that metabolic activation of BAT and recruitment of beige fat might have shared mechanisms. For example, beige fat cells emerge in response to administration of sympathomimetic agents, such as the β_3-adrenoreceptor agonist CL-316,243 (Collins et al., 1997), which also activates and expands BAT. Thus, like BAT, beige fat physiology is likely to be controlled by input from the sympathetic nervous system (Murano et al., 2009). However, the specific neural population(s) responsible for beige fat recruitment remain undefined.

To determine if central 5-HT neurons facilitate stimulation of beige fat cells, as they do BAT, we measured *Ucp1* and *Dio2* expression in subcutaneous inguinal WAT of $DTR^{f/f}ePet1^{Cre}$ and control mice, housed at 22°C, four days after DT-treatment. In DT-treated $DTR^{f/f}ePet1^{Cre}$ mice, *Ucp1* expression was 76% lower (0.24 ± 0.09 fold, n=6 vs 1.00 ± 0.12 fold, n=3 in controls; $P<0.002$), and *Dio2* expression was 84% lower (0.15 ± 0.07 fold, n=6 vs 1.00 ± 0.48 fold, n=3 in controls; $P<0.041$) than controls (Figure 5D and E). Thus, *Pet-1+* neurons are also important for driving expression of thermogenic genes in scWAT at 22°C, a temperature at which *Ucp1* expression in scWAT is ~20-fold higher than it is at 30°C (Qiu et al., 2014), which suggests ongoing sympathetic stimulation, even at mild temperatures.

Similarly, in mice where DT was delivered i.c.v., *Ucp1* expression in scWAT declined by 97% in $DTR^{f/f}ePet1^{Cre}$ mice (0.03 ± 0.01 fold, n=4 vs. 1.06 ± 0.23 fold, n=4 in controls; $P<0.0042$) four days after treatment. (Figure 5F).

Developmental loss of all CNS 5-HT neurons also reduces expression of thermogenic genes in both BAT and scWAT

To rule out unknown model-specific confounders that might have influenced our results, we also studied BAT and beige fat in $Lmx1b^{f/f}ePet1^{Cre}$ mice, which are deficient in CNS 5-HT neurons because they lack expression of a transcription factor essential for *Pet-1+* neuron development, LIM-homeodomain transcription factor 1b (*Lmx1b*) (Ding et al., 2003; Zhao et al., 2006). These mice exhibit increased mortality during early postnatal life. Surviving $Lmx1b^{f/f}ePet1^{Cre}$ mice maintain normal basal body temperature T_{core} at an ambient temperature of 22°C (Hodges et al., 2008), but have a severe thermoregulatory deficit when challenged with exposure to an ambient temperature of 16°C or 4°C. In these $Lmx1b^{f/f}ePet1^{Cre}$ mice, thermosensation and heat conservation mechanisms are intact, but there is impaired thermogenesis from shivering and, to a lesser extent, BAT activation upon transfer to 4°C (Hodges et al., 2008).

Consistent with results obtained in *DTR$^{f/f}$ePet1^{Cre}* mice, *Ucp1* expression was 25% lower in interscapular BAT of cold-challenged *Lmx1b$^{f/f}$ePet1^{Cre}* vs WT mice (1.01 ± 0.05, n=5 in WT vs 0.76 ± 0.10 in *Lmx1b$^{f/f}$ePet1^{Cre}*, n=5; P<0.05), and *Dio2* expression was 52% lower (1.03 ± 0.12, n=5 in WT vs 0.49 ± 0.05 in *Lmx1b$^{f/f}$ePet1^{Cre}*, n=5; P<0.005), demonstrating attenuated sympathetic activation of BAT in response to cold (Figure 5G and H). In scWAT, there was no difference in expression of *Ucp1* or *Dio2* mRNA in WT vs *Lmx1b$^{f/f}$ePet1^{Cre}* mice at an ambient temperature of 22°C. After exposure to an ambient temperature of 4°C, however, expression of *Ucp1* mRNA was induced 28-fold in scWAT of WT mice, but only 6.4-fold in *Lmx1b$^{f/f}$ePet1^{Cre}* animals (from 1.59 ± 0.93 to 44.81 ± 8.8 fold, n=3–5 in WT vs 2.24 ± 1.09 to 14.44 ± 5.4 fold in *Lmx1b$^{f/f}$ePet1^{Cre}*, n=3–5; P<0.004). Similarly, *Dio2* was induced by 28-fold in scWAT of WT mice (from 1.31 ± 0.52 to 36.99 ± 11.75 fold, n=3–5) vs 8.2-fold in *Lmx1b$^{f/f}$ePet1^{Cre}* mice (1.70 ± 0.51 to 13.81 ± 3.64 fold, n=3–5; P<0.04) (Figure 5I and J). Collectively, these data show, using a second *in vivo* model with different mechanisms, that the absence of central 5-HT neurons impairs sympathetic activation of brown and beige fat in response to cold.

Pet-1+ neuron projections to the spinal intermediolateral cell column are lost in DT-treated DTR$^{f/f}$ePet1^{Cre}mice

We examined tissue from mice expressing enhanced yellow fluorescent protein (EYFP) under control of the *Pet-1* enhancer region (*ePet*-EYFP mice) (Scott et al., 2005). Preganglionic sympathetic neurons (PSNs) of the intermediolateral horn (IML), which innervate BAT, receive projections from 5-HT neurons in the raphé pallidus and obscurus (Loewy, 1981). 5-HT excites PSNs in the IML, including those that control thermogenesis (Madden and Morrison, 2006, 2010). Therefore, we hypothesized that *Pet-1*+ neurons regulate BAT thermogenesis via projections to the IML. Using *ePet*-EYFP reporter mice, we identified EYFP+ cell bodies in the medulla and projections in the spinal cord (Figure 6A). There were dense projections to the IML of the thoracic spinal cord at levels T2–T5, as well as diffuse projections to the ventral and dorsal horns (Figure 6A). By contrast, EYFP+ projections were absent from BAT, liver, and pancreas, arguing against direct serotonergic innervation of these tissues. These data are consistent with the view that *Pet-1*+ cells influence thermogenesis by regulating sympathetic outflow to BAT and beige fat.

5-HT projections to the IML would be expected to be lost in DT-treated *DTR$^{f/f}$ePet1^{Cre}* mice, which cannot thermoregulate, and tissue 5-HT content should decrease. To test this, we harvested the thoracic spinal cord and raphé from DT-treated *DTR$^{f/f}$ePet1^{Cre}* and control mice for histology and HPLC. As expected, destruction of *Pet-1*+ neurons reduced raphé 5-HT content by 50% (0.019 ± 0.002 ng/mg, n=6 in DT-treated *DTR$^{f/f}$ePet1^{Cre}* vs. 0.039 ± 0.002 ng/mg, n=6 in controls; P<0.005) and thoracic spinal 5-HT content by 52% (0.348 ± 0.067 ng/mg, n=5 in DT-treated *DTR$^{f/f}$ePet1^{Cre}* vs. 0.724 ± 0.142 ng/mg, n=5 in controls; P<0.045) (Figure 6G and H). Similarly, 5-HT was reduced by 93% in spinal cords of *Lmx1b$^{f/f}$ePet1^{Cre}* mice (0.037 ± 0.013 ng/mg, n=3) compared to controls (0.568 ± 0.007 ng/mg, n=3; P<0.0001) (Figure 6I).

We also sectioned spinal cords from these mice, staining for expression of the serotonin transporter (Slc6a4), a marker of 5-HT neuron terminals, in the IML. Slc6a4 staining in the

IML was reduced by 73% in DT-treated *DTR$^{f/f}$ePet1^{Cre}* mice (817.8 ± 89.81 integrated density, n=6) compared to controls (220.8 ± 58.01 integrated density, n=5; P<0.0003) (Figure 6B–F).

Discussion

Here we report that deletion of central 5-HT neurons in mice causes steatosis of BAT, impaired browning of WAT, and loss of thermoregulation. These effects are accompanied by decreased expression of genes essential for thermogenesis in BAT and beige fat, including *Ucp1*. Furthermore, deletion of central 5-HT neurons causes severe hyperglycemia and hyperlipidemia that are only partially attributable to the observed defects in BAT. These results indicate that 5-HT neurons facilitate sympathetic drive to BAT, promote browning of scWAT, and maintain normal levels of metabolic energy substrates in blood. Central serotonergic neurons may be master regulators of whole body energy homeostasis. This role may be intertwined with a larger role integrating metabolism, body temperature and breathing, explaining the contribution of these neurons to central CO_2 chemoreception (Brust et al., 2014; Hodges et al., 2008, 2011; Ray et al., 2011).

Serotonergic neurons are essential for normal thermogenesis and have been proposed to play a role in facilitating BAT activity (Nakamura and Morrison, 2011; Nakamura et al., 2004), but they have not been linked to maintaining the phenotype of BAT or to browning of scWAT. Rather, the predominant focus on BAT activation has been on noradrenergic signaling, possibly through interaction with peripheral hematopoetic cells (Qiu et al., 2014; Rao et al., 2014). Thus, our work provides direct evidence that central 5-HT neurons are required for thermogenesis by brown and beige adipocytes.

Prior work has suggested that 5-HT neurons also contribute to metabolic homeostasis. For example, 5-HT influences glucose metabolism and appetite through an incompletely delineated mechanism involving the sympathetic nervous system (Lam and Heisler, 2007). Lorcaserin, a $5HT_{2C}$ receptor agonist, reduces body weight and improves glycemic control, and was recently approved to treat human obesity (O'Neil et al., 2012), while genetic deletion of the $5\text{-}HT_{2C}$ receptor in mice leads to obesity (Tecott et al., 1995). Further data show that selective deletion of $5\text{-}HT_{2C}$ receptors in pre-opiomelanocortin (POMC) neurons, part of a circuit which may be impacted in our 5-HT deletion models, negatively alters glucoregulation (Berglund et al., 2013). Some effects of 5-HT on metabolism are independent of changes in body weight. For example, at doses that do not alter food intake, $5\text{-}HT_{2C}$ receptor agonists reduce hepatic glucose production and improve glucose homeostasis in mice, while $5\text{-}HT_{2C}$ receptor antagonists cause hyperglycemia (Xu et al., 2010; Zhou et al., 2007). The current findings suggest that serotonergic and other neuron types in the CNS play a greater role in control of peripheral nutrient metabolism than has been fully appreciated (Schwartz et al., 2013). This effect is likely mediated by both sympathetic projections to BAT, as well as sympathetic projections to beige fat and to the liver.

Reduced substrate oxidation in BAT and beige fat is one mechanism that may contribute to metabolic dysfunction in models of reduced brain 5-HT. However, the persistence of

hyperglycemia in 5-HT neuron ablated animals housed at a thermoneutral ambient temperature suggests that at least some aspects of 5-HT neuron-mediated control of glucose homeostasis are independent of brown or beige fat. We considered at least four potential mechanisms of this BAT-independent hyperglycemia. First, 5-HT neurons modulate pancreatic insulin production, as mice treated systemically with DT were hypoinsulinemic. However, though clearly important, this mechanism does not appear to be sufficient to explain our observations, as i.c.v. DT-treated mice have normal insulin levels, but remain severely hyperglycemic. A second hypothesis is that 5-HT neurons modulate hepatic glucose production or peripheral insulin sensitivity. Thirdly, 5-HT neurons may simply modulate glycemic control through other critical endocrine modulators of metabolism, such as corticosteroids and the thyroid axis. Finally, recent evidence in humans shows that the greatest glucose utilization in response to acute cold is by deep proximal muscles rather than by brown adipocytes (Blondin et al., 2015). As shivering is impaired in $Lmx1b^{f/f}ePet1^{Cre}$ mice in response to cold (Hodges et al., 2008), it may be that the 5-HT neuron ablated $DTR^{f/f}ePet1^{Cre}$ mice also have impaired glucose utilization from skeletal muscle, partially explaining the exaggerated hyperglycemia in these animals. Our data suggest that all four of these non-BAT mechanisms may be involved in mediating this response.

5-HT neurons are heterogeneous (Brust et al., 2014), and further work will be required to identify the subpopulation(s) of *Pet-1*+ neurons responsible for activating BAT and/or controlling glucose metabolism. Based on prior studies, we believe selective control of these processes is likely. For example, sibutramine, which blocks 5-HT and NE uptake, increases brown fat activity 18-fold in rats, without affecting metabolism of other tissues (Connoley et al., 1999). Similarly, cold-evoked vasoconstriction in the tail, a mechanism that contributes significantly to heat conservation in mice, is not affected in $Pet\text{-}1^{-/-}$ or $Lmx1b^{f/f}ePet1^{Cre}$ animals (Cummings et al., 2011; Hodges et al., 2008).

Beyond the populations of *Pet-1*+ neurons that impart these effects, many questions remain unanswered about the mechanism by which these 5-HT neurons function. For example, it will be important to determine whether 5-HT activates thermogenesis itself, or alternatively acts as a permissive or neuromodulatory signal for other central activators of sympathetic discharge. For example, *Pet-1*+ neurons could modify activity (or alter responsiveness to glutamate) of PSNs in the spinal cord IML that are important for sympathetic discharge in interscapular and subcutaneous adipose tissue. Such a mechanism would determine whether increased serotonergic tone could supraphysiologically enhance BAT activity, or whether loss of 5-HT tone could reduce BAT activity.

In summary, we have identified *Pet-1*+ neurons as indispensable for sympathetic activation of adult mouse brown and beige/brite adipose tissue, for maintenance of their “brown” phenotype, and for thermogenesis in BAT. We also have shown that *Pet-1*+ neurons are necessary for maintaining homeostatic circulating levels of glucose and lipids. This latter effect is due in part to effects on BAT substrate oxidation, although it is likely that generation of glucose by the liver also plays an important role. This work identifies a subset of *Pet-1*+ neurons as key regulators of diverse metabolic processes, and therefore as potential targets for treatment of obesity and type 2 diabetes, in part by activation of BAT.

EXPERIMENTAL PROCEDURES

Animals

All animal experiments were performed according to procedures approved by The University of Iowa Institutional Animal Care and Use Committee. Sex and age-matched mice were maintained on a standard laboratory chow on a 12-hour light and dark cycle. WT mice injected with DT exhibit no temperature phenotype or differences in gene expression relative to PBS-injected $DTR^{f/f}ePet1^{Cre}$ mice in any tissue. Thus, for the experiments described below, littermate PBS-injected $DTR^{f/f}ePet1^{Cre}$ mice were used as controls in testing the effects of CNS-Cre expression, *Pet-1+* cell expression of the human diphtheria-toxin receptor, and the mixed genetic background. DT (Sigma Aldrich) was injected intraperitoneally at a concentration of 2.250 μg/mouse. For i.c.v. injections, canulas from Alzet brain infusion kit 3 (DURECT corporation, Cupertino, CA 95014) were used. Following ketamine (87mg/kg)/xylazine (13mg/kg) anaesthesia, mice were placed in a stereotaxic apparatus, and the injection guide canula was inserted using the following coordinates: 0.2mm caudal to bregma, 1.0mm later to midline, 2.5mm below skull surface.

Temperature Measurements

BMDS electronic ID transponders (Bio Medic Data Systems, Inc.) were implanted subcutaneously into the intrascapular region of mice 2–4 months of age for temperature measurements. Baseline temperature (T_{BAT}) was measured for 5 days prior to injection, and T_{BAT} was measured for 4 days following injection.

Real-time Quantitative PCR Analysis

Animals used for transcription analysis were 6.5–8 months of age. BAT RNA was extracted using the standard TRIzol-chloroform method, following the manufacturer's instructions (Ambion). Inguinal WAT RNA was extracted using the RNeasy Mini Kit (Qiagen). mRNA was reverse transcribed using the Qiagen Quantitect Reverse Transcription Kit, with quality assessed using a Nanodrop 1000. Quantitative PCR reactions contained *Power* SYBR green fluorescent dye from Applied Biosystems, and measurements were made using an Agilent MX3000P system. Relative mRNA expression for the $DTR^{f/f}ePet1^{Cre}$ mice was determined following normalization to β-actin levels using the ΔΔ-CT method. Relative mRNA expression for the $Lmx1b^{f/f}ePet1^{Cre}$ mice was determined following normalization to GAPDH levels using the ΔΔ-CT method. Taqman Gene Expression Assays were used for *Pet-1(Fev) (Assay ID: Mm00462220_m1) and Hbegf (Assay ID: Hs00181813_m1)*.

Sequences of UCP1 Primers (5'→ 3'):

Forward: ACG TCC CCT GCC ATT TAC TGT CA

Reverse: GGC CGT CGG TCC TTC CTT

Sequences of DIO2 Primers (5'→ 3'):

Forward: TCT GTA GCC CCG AAT TCC CAA GTG

Reverse: TCC CAG CTG TGT ACA TGC CTC AAT

Sequences of β-Actin Primers(5'→ 3'):

Forward: GGC TGT ATT CCC CTC CAT CG

Reverse: CCA GTT GGT AAC AAT GCC ATG T

Sequences of GAPDH Primers (5' → 3'):

Forward: CTG ACG TGC CGC CTG GAG AAA

Reverse: CCC GGC ATC GAA GGT GGA AGA GT

Genotyping Primers (5' → 3'):

***Lmx1b$^{f/f}$ePet1^{Cre}* mice**:

Flox1: AGG CTC CAT CCA TTC TTC TC

Flox2: CCA CAA TAA GCA AGA GGC AC

Cre1: ATT TGC CTG CAT TAC CGG TCG

Cre2: CAG CAT TGC TGT CAC TTG GTC

***DTR$^{f/f}$ePet1^{Cre}* mice**:

DTR Forward: ACC ATG AAG CTG CTG CCG TC

DTR Reverse: ATC AGT GGG AAT TAG TCA TGC

Cre1: ATT TGC CTG CAT TAC CGG TCG

Cre2: CAG CAT TGC TGT CAC TTG GTC

Confocal Imaging

Animals were anesthetized using ketamine (87mg/kg)/xylazine (13mg/kg) and perfused with PBS followed by 4% paraformaldehyde (PFA). Following resection of the brain and spinal column, tissues were placed in 4% PFA overnight. Thoracic sections were stained using an anti-SERT (SLC6A4) rabbit polyclonal primary antibody (ab44520) at a concentration of 1:500 overnight at 4°C, obtained from Abcam (Abcam plc, Cambridge, MA 02139). The sections were then subsequently stained at 4°C for 1 hour using Alexa-Fluor 488 goat anti-rabbit secondary antibody (BD Biosciences, San Jose, CA 95131).Tissue slices were then coverslipped using Vectashield mounting medium containing DAPI (Vector Labs, Inc., Burlingame, CA 94010).

Histology

BAT from mice 2–7 months of age was extracted immediately following euthanasia under isofluorane anesthesia. Tissue was placed in 4% PFA for 24 hours, followed by PBS. Tissue was then paraffin embedded and stained using Hematoxylin and Eosin (H&E) at the University of Iowa Histology Research Core. Images were collected using a Leica Microsystems DMI-6000B inverted microscope. Lipid droplets were quantified using the MRI Adipocyte Tools with ImageJ software.

Plasma Serum Harvest and Biomarker Measurement

Blood was extracted from ad libitum fed mice 2–6 months of age via cardiac puncture under isofluorane following one hour acclimatization period, at minimum. Extractions were performed near end of the light cycle. Blood was immediately centrifuged at 3,000 g for 5 min at 4°C, to separate plasma from blood cells. Plasma fatty acids were measured using the HR Series NEFA-HR kit (Wako Diagnostics). Plasma triglycerides were measured using the Infinity Triglyceride Reagent (Thermoscientific). Blood glucose was measured using an AlphaTrak glucose meter and blood glucose test strips (Abbott Laboratories). Plasma ketones were measured using a Ketone Body Assay Kit (Abnova Corporation). Plasma corticosterone, TSH, and insulin were measured using radioimmunoassay and quantified using a Packard Gamma counter, by the Vanderbilt Hormone Assay and Analytical Services Core, Vanderbilt University, Nashville, TN 37232.

Cold Exposure

Animals used for cold exposure experiments were 2–3 months of age. Animals in normal cages with bedding were placed in a 4°C room for four hours, and were inspected every 30 min during this period to ensure they were alive. As we had previously shown that T_{core} of *Lmx1b*$^{f/f}$*ePet1*^{Cre} mice drops to lethal levels after two hours of 4°C exposure (Hodges et al., 2008), those that became immobile were moved to room temperature and euthanized under isofluorane, where the interscapular BAT and inguinal WAT were resected. For each timepoint at which an *Lmx1b*$^{f/f}$*ePet1*^{Cre} mouse was euthanized, a WT mouse was also euthanized. The five timepoints were as follows: 2.5 hrs, 3 hrs, 3.5 hrs, 4 hrs, 4.5 hrs.

Statistical Methods

Data-set statistics were analyzed using the GraphPad Prism software, version 6.01. The Student's t-test was used to compare data sets. Data are represented as the mean ± SEM.

Supplementary Material

Refer to Web version on PubMed Central for supplementary material.

Acknowledgements

We are grateful to Xiuqiong Zhou for mouse breeding and genotyping and Lori A. Smith for technical assistance. Thanks to Michael Jurczak, Zachary Gerhart- Hines, Kitt Falk Petersen, Maja Lind Rasmussen, Randi Bonke Mikkelsen, Mathias Falkerslev, Cory A. Massey, and Lola Torz for helpful comments. This work was supported by the University of Iowa Department of Neurology, the Novo Nordisk Foundation Center for Basic Metabolic Research, the Danish Research Council, and the Lundbeck Foundation. M.J.P. is funded by an American Diabetes Association Junior Faculty Award 7-13-JF-49 and an Edward Mallinckrodt Jr. Foundation Grant. K.R.M is supported by NIH F32DK102347. The Hormone Assay and Analytical Services Core is supported by NIH grants DK059637 and DK020593.

References

Bartelt A, Bruns OT, Reimer R, Hohenberg H, Ittrich H, Peldschus K, Kaul MG, Tromsdorf UI, Weller H, Waurisch C, et al. Brown adipose tissue activity controls triglyceride clearance. Nat. Med. 2011; 17:200–205. [PubMed: 21258337]

Berglund ED, Liu C, Sohn JW, Liu T, Kim MH, Lee CE, Vianna CR, Williams KW, Xu Y, Elmquist JK. Serotonin 2C receptors in pro-opiomelanocortin neurons regulate energy and glucose homeostasis. J. Clin. Invest. 2013; 123:5061–5070. [PubMed: 24177424]

Beviz A, Lundholm L, Mohme-Lundholm E. Cyclic AMP as a mediator of hormonal metabolic effects in brown adipose tissue. Br. J. Pharmacol. 1968; 34:198P–199P.

Blondin DP, Labbé SM, Phoenix S, Guérin B, Turcotte ÉE, Richard D, Carpentier AC, Haman F. Contributions of white and brown adipose tissues and skeletal muscles to acute cold-induced metabolic responses in healthy men. J. Physiol. 2015; 593:701–714. [PubMed: 25384777]

Boyer EW, Shannon M. The serotonin syndrome. N. Engl. J. Med. 2005; 352:1112–1120. [PubMed: 15784664]

Brust RD, Corcoran AE, Richerson GB, Nattie E, Dymecki SM. Functional and Developmental Identification of a Molecular Subtype of Brain Serotonergic Neuron Specialized to Regulate Breathing Dynamics. Cell Rep. 2014; 9:2152–2165. [PubMed: 25497093]

Buch T, Heppner FL, Tertilt C, Heinen TJAJ, Kremer M, Wunderlich FT, Jung S, Waisman A. A Cre-inducible diphtheria toxin receptor mediates cell lineage ablation after toxin administration. Nat. Methods. 2005; 2:419–426. [PubMed: 15908920]

Cameron IL, Smith RE. Cytological Responses of Brown Fat Tissue in Cold-exposed rats. J. Cell Biol. 1964; 23:89–100. [PubMed: 14228521]

Cannon B, Nedergaard J. Brown adipose tissue: function and physiological significance. Physiol. Rev. 2004; 84:277–359. [PubMed: 14715917]

Cano G, Passerin AM, Schiltz JC, Card JP, Morrison SF, Sved AF. Anatomical substrates for the central control of sympathetic outflow to interscapular adipose tissue during cold exposure. J. Comp. Neurol. 2003; 460:303–326. [PubMed: 12692852]

Cerpa V, Gonzalez A, Richerson GB. Diphtheria toxin treatment of Pet-1-Cre floxed diphtheria toxin receptor mice disrupts thermoregulation without affecting respiratory chemoreception. Neuroscience. 2014

Cohade C, Osman M, Pannu HK, Wahl RL. Uptake in supraclavicular area fat ("USA-Fat"): description on 18F-FDG PET/CT. J. Nucl. Med. Off. Publ. Soc. Nucl. Med. 2003; 44:170–176.

Cohen P, Levy JD, Zhang Y, Frontini A, Kolodin DP, Svensson KJ, Lo JC, Zeng X, Ye L, Khandekar MJ, et al. Ablation of PRDM16 and Beige Adipose Causes Metabolic Dysfunction and a Subcutaneous to Visceral Fat Switch. Cell. 2014; 156:304–316. [PubMed: 24439384]

Collins S, Daniel KW, Petro AE, Surwit RS. Strain-specific response to beta 3-adrenergic receptor agonist treatment of diet-induced obesity in mice. Endocrinology. 1997; 138:405–413. [PubMed: 8977430]

Connoley IP, Liu YL, Frost I, Reckless IP, Heal DJ, Stock MJ. Thermogenic effects of sibutramine and its metabolites. Br. J. Pharmacol. 1999; 126:1487–1495. [PubMed: 10217544]

Cummings KJ, Li A, Nattie EE. Brainstem serotonin deficiency in the neonatal period: autonomic dysregulation during mild cold stress. J. Physiol. 2011; 589:2055–2064. [PubMed: 21486799]

Cypess AM, Lehman S, Williams G, Tal I, Rodman D, Goldfine AB, Kuo FC, Palmer EL, Tseng Y-H, Doria A, et al. Identification and importance of brown adipose tissue in adult humans. N. Engl. J. Med. 2009; 360:1509–1517. [PubMed: 19357406]

Cypess AM, Chen Y-C, Sze C, Wang K, English J, Chan O, Holman AR, Tal I, Palmer MR, Kolodny GM, et al. Cold but not sympathomimetics activates human brown adipose tissue in vivo. PNAS. 2012; 109:10001–10005. [PubMed: 22665804]

Ding Y-Q, Marklund U, Yuan W, Yin J, Wegman L, Ericson J, Deneris E, Johnson RL, Chen Z-F. Lmx1b is essential for the development of serotonergic neurons. Nat. Neurosci. 2003; 6:933–938. [PubMed: 12897786]

Enerbäck S, Jacobsson A, Simpson EM, Guerra C, Yamashita H, Harper ME, Kozak LP. Mice lacking mitochondrial uncoupling protein are cold-sensitive but not obese. Nature. 1997; 387:90–94. [PubMed: 9139827]

English JT, Patel SK, Flanagan MJ. Association of Pheochromocytomas with Brown Fat Tumors. Radiology. 1973; 107:279–281. [PubMed: 4695890]

Fuller NJ, Stirling DM, Dunnett S, Reynolds GP, Ashwell M. Decreased brown adipose tissue thermogenic activity following a reduction in brain serotonin by intraventricular p-chlorophenylalanine. Biosci. Rep. 1987; 7:121–127. [PubMed: 2443195]

Gerhart-Hines Z, Feng D, Emmett MJ, Everett LJ, Loro E, Briggs ER, Bugge A, Hou C, Ferrara C, Seale P, et al. The nuclear receptor Rev-erbα controls circadian thermogenic plasticity. Nature. 2013; 503:410–413. [PubMed: 24162845]

Harms M, Seale P. Brown and beige fat: development, function and therapeutic potential. Nat. Med. 2013; 19:1252–1263. [PubMed: 24100998]

Hodges MR, Tattersall GJ, Harris MB, McEvoy SD, Richerson DN, Deneris ES, Johnson RL, Chen Z-F, Richerson GB. Defects in breathing and thermoregulation in mice with near-complete absence of central serotonin neurons. J. Neurosci. 2008; 28:2495–2505. [PubMed: 18322094]

Hodges MR, Best S, Richerson GB. Altered ventilatory and thermoregulatory control in male and female adult Pet-1 null mice. Respir. Physiol. Neurobiol. 2011; 177:133–140. [PubMed: 21453797]

Hsieh AC, Carlson LD. Role of adrenaline and noradrenaline in chemical regulation of heat production. Am. J. Physiol. 1957; 190:243–246. [PubMed: 13458448]

Huttunen P, Hirvonen J, Kinnula V. The occurrence of brown adipose tissue in outdoor workers. Eur. J. Appl. Physiol. Occup. Physiol. 1981; 46:339–345. [PubMed: 6266825]

Jespersen NZ, Larsen TJ, Peijs L, Daugaard S, Homøe P, Loft A, de Jong J, Mathur N, Cannon B, Nedergaard J, et al. A Classical Brown Adipose Tissue mRNA Signature Partly Overlaps with Brite in the Supraclavicular Region of Adult Humans. Cell Metab. 2013; 17:798–805. [PubMed: 23663743]

Kajimura S, Saito M. A New Era in Brown Adipose Tissue Biology: Molecular Control of Brown Fat Development and Energy Homeostasis. Annu. Rev. Physiol. 2014; 76:225–249. [PubMed: 24188710]

Lam DD, Heisler LK. Serotonin and energy balance: molecular mechanisms and implications for type 2 diabetes. Expert Rev. Mol. Med. 2007; 9:1–24. [PubMed: 17316471]

Loewy AD. Raphe pallidus and raphe obscurus projections to the intermediolateral cell column in the rat. Brain Res. 1981; 222:129–133. [PubMed: 6170384]

Madden CJ, Morrison SF. Serotonin potentiates sympathetic responses evoked by spinal NMDA. J. Physiol. 2006; 577:525–537. [PubMed: 16973701]

Madden CJ, Morrison SF. Endogenous activation of spinal 5-hydroxytryptamine (5-HT) receptors contributes to the thermoregulatory activation of brown adipose tissue. Am. J. Physiol. Regul. Integr. Comp. Physiol. 2010; 298:R776–R783. [PubMed: 20071609]

Van Marken Lichtenbelt WD, Vanhommerig JW, Smulders NM, Drossaerts JMAFL, Kemerink GJ, Bouvy ND, Schrauwen P, Teule GJJ. Cold-activated brown adipose tissue in healthy men. N. Engl. J. Med. 2009; 360:1500–1508. [PubMed: 19357405]

Morrison SF. RVLM and raphe differentially regulate sympathetic outflows to splanchnic and brown adipose tissue. Am. J. Physiol. - Regul. Integr. Comp. Physiol. 1999; 276:R962–R973.

Morrison S, Madden CJ, Tupone D. Central Neural Regulation of Brown Adipose Tissue Thermogenesis and Energy Expenditure. Cell Metab. 2014; 19:741–756. [PubMed: 24630813]

Murano I, Barbatelli G, Giordano A, Cinti S. Noradrenergic parenchymal nerve fiber branching after cold acclimatisation correlates with brown adipocyte density in mouse adipose organ. J. Anat. 2009; 214:171–178. [PubMed: 19018882]

Nakamura K, Morrison SF. Central efferent pathways for cold-defensive and febrile shivering. J. Physiol. 2011; 589:3641–3658. [PubMed: 21610139]

Nakamura K, Matsumura K, Hübschle T, Nakamura Y, Hioki H, Fujiyama F, Boldogköi Z, König M, Thiel H-J, Gerstberger R, et al. Identification of sympathetic premotor neurons in medullary raphe regions mediating fever and other thermoregulatory functions. J. Neurosci. 2004; 24:5370–5380. [PubMed: 15190110]

Nason MW, Mason P. Medullary raphe neurons facilitate brown adipose tissue activation. J. Neurosci. 2006; 26:1190–1198. [PubMed: 16436606]

Nedergaard J, Cannon B. The Browning of White Adipose Tissue: Some Burning Issues. Cell Metab. 2014; 20:396–407. [PubMed: 25127354]

Nedergaard J, Bengtsson T, Cannon B. Unexpected evidence for active brown adipose tissue in adult humans. Am. J. Physiol. - Endocrinol. Metab. 2007; 293:E444–E452. [PubMed: 17473055]

Nedergaard J, Bengtsson T, Cannon B. New Powers of Brown Fat: Fighting the Metabolic Syndrome. Cell Metab. 2011; 13:238–240. [PubMed: 21356513]

Nguyen NLT, Randall J, Banfield BW, Bartness TJ. Central sympathetic innervations to visceral and subcutaneous white adipose tissue. Am. J. Physiol. Regul. Integr. Comp. Physiol. 2014; 306:R375–R386. [PubMed: 24452544]

O'Neil PM, Smith SR, Weissman NJ, Fidler MC, Sanchez M, Zhang J, Raether B, Anderson CM, Shanahan WR. Randomized Placebo-Controlled Clinical Trial of Lorcaserin for Weight Loss in Type 2 Diabetes Mellitus: The BLOOM-DM Study. Obesity. 2012; 20:1426–1436. [PubMed: 22421927]

Ohta Y, Kosaka Y, Kishimoto N, Wang J, Smith SB, Honig G, Kim H, Gasa RM, Neubauer N, Liou A, et al. Convergence of the insulin and serotonin programs in the pancreatic β-cell. Diabetes. 2011; 60:3208–3216. [PubMed: 22013016]

Qiu Y, Nguyen KD, Odegaard JI, Cui X, Tian X, Locksley RM, Palmiter RD, Chawla A. Eosinophils and Type 2 Cytokine Signaling in Macrophages Orchestrate Development of Functional Beige Fat. Cell. 2014; 157:1292–1308. [PubMed: 24906148]

Rao RR, Long JZ, White JP, Svensson KJ, Lou J, Lokurkar I, Jedrychowski MP, Ruas JL, Wrann CD, Lo JC, et al. Meteorin-like Is a Hormone that Regulates Immune-Adipose Interactions to Increase Beige Fat Thermogenesis. Cell. 2014; 157:1279–1291. [PubMed: 24906147]

Ray RS, Corcoran AE, Brust RD, Kim JC, Richerson GB, Nattie E, Dymecki SM. Impaired respiratory and body temperature control upon acute serotonergic neuron inhibition. Science. 2011; 333:637–642. [PubMed: 21798952]

Rother E, Belgardt BF, Tsaousidou E, Hampel B, Waisman A, Myers MG, Brüning JC. Acute selective ablation of rat insulin promoter-expressing (RIPHER) neurons defines their orexigenic nature. PNAS. 2012; 109:18132–18137. [PubMed: 23064638]

Schwartz MW, Seeley RJ, Tschöp MH, Woods SC, Morton GJ, Myers MG, D'Alessio D. Cooperation between brain and islet in glucose homeostasis and diabetes. Nature. 2013; 503:59–66. [PubMed: 24201279]

Scott MM, Wylie CJ, Lerch JK, Murphy R, Lobur K, Herlitze S, Jiang W, Conlon RA, Strowbridge BW, Deneris ES. A genetic approach to access serotonin neurons for in vivo and in vitro studies. PNAS. 2005; 102:16472–16477. [PubMed: 16251278]

Shabalina IG, Petrovic N, de Jong JMA, Kalinovich AV, Cannon B, Nedergaard J. UCP1 in brite/beige adipose tissue mitochondria is functionally thermogenic. Cell Rep. 2013; 5:1196–1203. [PubMed: 24290753]

Smith JE, Jansen ASP, Gilbey MP, Loewy AD. CNS cell groups projecting to sympathetic outflow of tail artery: neural circuits involved in heat loss in the rat. Brain Res. 1998; 786:153–164. [PubMed: 9554992]

Söderlund V, Larsson SA, Jacobsson H. Reduction of FDG uptake in brown adipose tissue in clinical patients by a single dose of propranolol. Eur. J. Nucl. Med. Mol. Imaging. 2007; 34:1018–1022. [PubMed: 17225118]

Strack AM, Sawyer WB, Platt KB, Loewy AD. CNS cell groups regulating the sympathetic outflow to adrenal gland as revealed by transneuronal cell body labelling with pseudorabies virus. Brain Res. 1989; 491:274–296. [PubMed: 2548665]

Tanuma Y, Ohata M, Ito T, Yokochi C. Possible function of human brown adipose tissue as suggested by observation on perirenal brown fats from necropsy cases of variable age groups. Arch. Histol. Jpn. 1976; 39:117–145. [PubMed: 962510]

Tecott LH, Sun LM, Akana SF, Strack AM, Lowenstein DH, Dallman MF, Julius D. Eating disorder and epilepsy in mice lacking 5-HT2c serotonin receptors. Nature. 1995; 374:542–546. [PubMed: 7700379]

Thomas SA, Palmiter RD. Thermoregulatory and metabolic phenotypes of mice lacking noradrenaline and adrenaline. Nature. 1997; 387:94–97. [PubMed: 9139828]

Virtanen KA, Lidell ME, Orava J, Heglind M, Westergren R, Niemi T, Taittonen M, Laine J, Savisto N-J, Enerbäck S, et al. Functional brown adipose tissue in healthy adults. N. Engl. J. Med. 2009; 360:1518–1525. [PubMed: 19357407]

Wu J, Cohen P, Spiegelman BM. Adaptive thermogenesis in adipocytes: Is beige the new brown? Genes Dev. 2013; 27:234–250. [PubMed: 23388824]

Xu Y, Berglund ED, Sohn J-W, Holland WL, Chuang J-C, Fukuda M, Rossi J, Williams KW, Jones JE, Zigman JM, et al. 5-HT2CRs expressed by pro-opiomelanocortin neurons regulate insulin sensitivity in liver. Nat. Neurosci. 2010; 13:1457–1459. [PubMed: 21037584]

Yoneshiro T, Aita S, Matsushita M, Kayahara T, Kameya T, Kawai Y, Iwanaga T, Saito M. Recruited brown adipose tissue as an antiobesity agent in humans. J. Clin. Invest. 2013; 123:3404–3408. [PubMed: 23867622]

Zhao J, Unelius L, Bengtsson T, Cannon B, Nedergaard J. Coexisting beta-adrenoceptor subtypes: significance for thermogenic process in brown fat cells. Am. J. Physiol. - Cell Physiol. 1994; 267:C969–C979.

Zhao Z-Q, Scott M, Chiechio S, Wang J-S, Renner KJ, Gereau RW, Johnson RL, Deneris ES, Chen Z-F. Lmx1b is required for maintenance of central serotonergic neurons and mice lacking central serotonergic system exhibit normal locomotor activity. J. Neurosci. 2006; 26:12781–12788. [PubMed: 17151281]

Zhou L, Sutton GM, Rochford JJ, Semple RK, Lam DD, Oksanen LJ, Thornton-Jones ZD, Clifton PG, Yueh C-Y, Evans ML, et al. Serotonin 2C receptor agonists improve type 2 diabetes via melanocortin-4 receptor signaling pathways. Cell Metab. 2007; 6:398–405. [PubMed: 17983585]

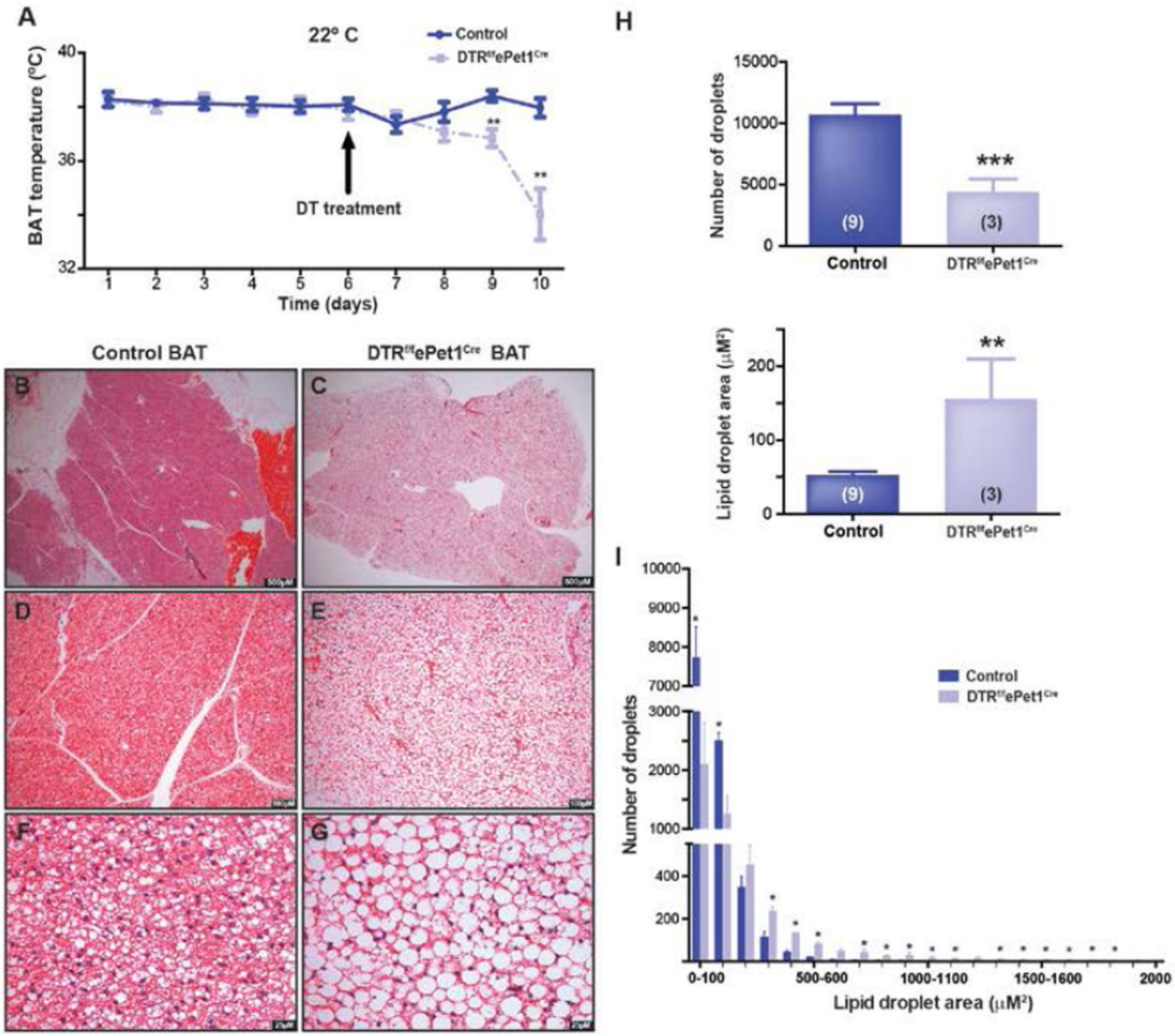

Figure 1. Ablation of *Pet-1*+ neurons impairs BAT thermogenesis and causes BAT steatosis

(A) BAT temperature (T_{BAT}) in i.p. DT-treated *DTR$^{f/f}$ePet1^{Cre}* mice. In *DTR$^{f/f}$ePet1^{Cre}* mice, T_{BAT} decreases after i.p. injection of diphtheria toxin (n = 6–7 mice/group).

(B) Control interscapular brown adipose tissue at 25× magnification, stained with H&E.

(C) Lipid accumulation in the cytosol of interscapular brown adipocytes in i.p. DT-treated *DTR$^{f/f}$ePet1^{Cre}* mice at 25× magnification, stained with H&E.

(D) Control brown adipose tissue at 100× magnification.

(E) Brown adipose tissue in i.p. DT-treated *DTR$^{f/f}$ePet1^{Cre}* mice at 100× magnification.

(F) Control brown adipose tissue at 400× magnification.

(G) Brown adipose tissue in i.p. DT-treated *DTR$^{f/f}$ePet1^{Cre}* mice at 400× magnification.

(H) Quantification of lipid droplet number and area in i.p. DT-treated *DTR$^{f/f}$ePet1^{Cre}* mice and controls.

(I) Lipid droplet size distribution in brown adipocytes from control and i.p. DT-treated *DTR*$^{f/f}$*ePet1*^{Cre} mice. Data are presented as mean ± SEM. *p < 0.05, **p < 0.01, ***p < 0.005.

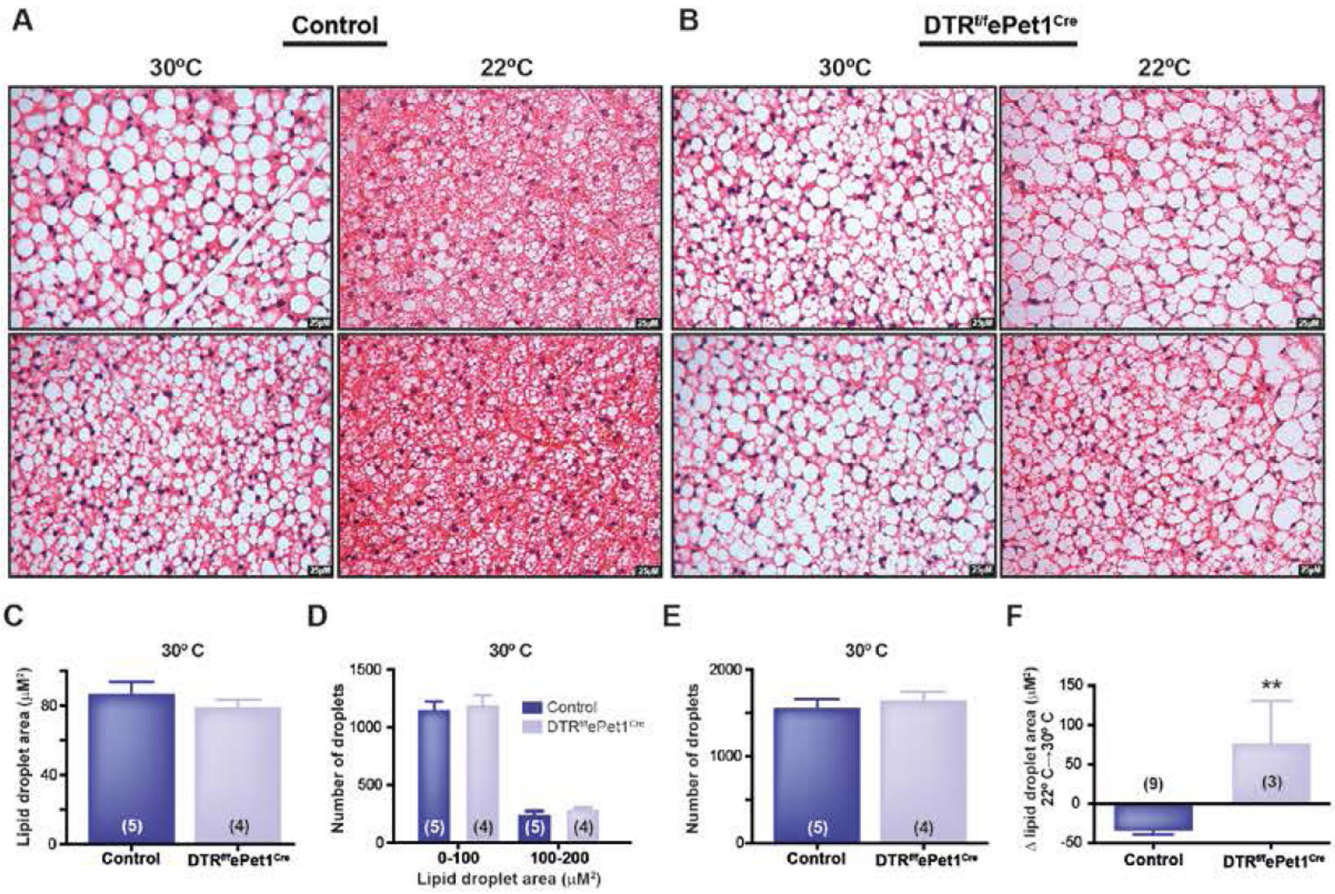

Figure 2. Mild cold exposure decreases lipid content in control BAT, but not *Pet-1*+ neuron-deficient mouse BAT

(A) Control BAT at 30°C and 22°C.

(B) i.p. DT-treated $DTR^{f/f}ePet1^{Cre}$ BAT at 30°C and 22°C.

(C) Similar lipid droplet area in control and i.p. DT-treated $DTR^{f/f}ePet1^{Cre}$ BAT at 30°C.

(D) Similar number of small lipid droplets in control and DT-treated $DTR^{f/f}ePet1^{Cre}$ mice at 30°C.

(E) Similar number of lipid droplets per field in control and DT-treated $DTR^{f/f}ePet1^{Cre}$ mice at 30°C.

(F) Change in lipid droplet area between 30°C and 22°C in control and in DT-treated $DTR^{f/f}ePet1^{Cre}$ mice.

Data are presented as mean ± SEM. *p < 0.05, **p < 0.01, ***p < 0.005, ****p < 0.001.

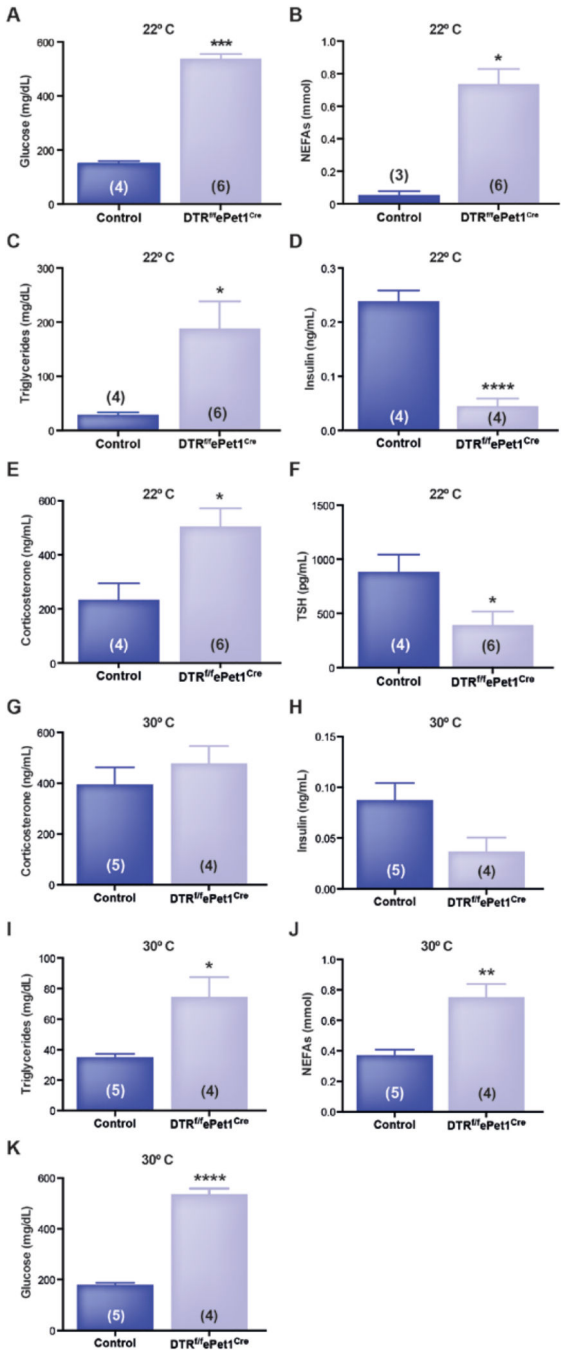

Figure 3. Ablation of *Pet-1*+ neurons causes hyperglycemia, hyperlipidemia, and endocrine changes that are partly temperature-dependent

(A–F) Plasma (A) glucose, (B) fatty acids, (C) triglycerides, (D) insulin, (E) corticosterone, (F) and thyroid-stimulating hormone in i.p. DT-treated DTRf/fePet1Cre mice and controls at 22°C.

(G–K) Plasma (G) corticosterone, (H) insulin, (I) triglycerides, (J) fatty acids, and (K) glucose in DT-treated DTRf/fePet1Cre mice and controls at 30°C.

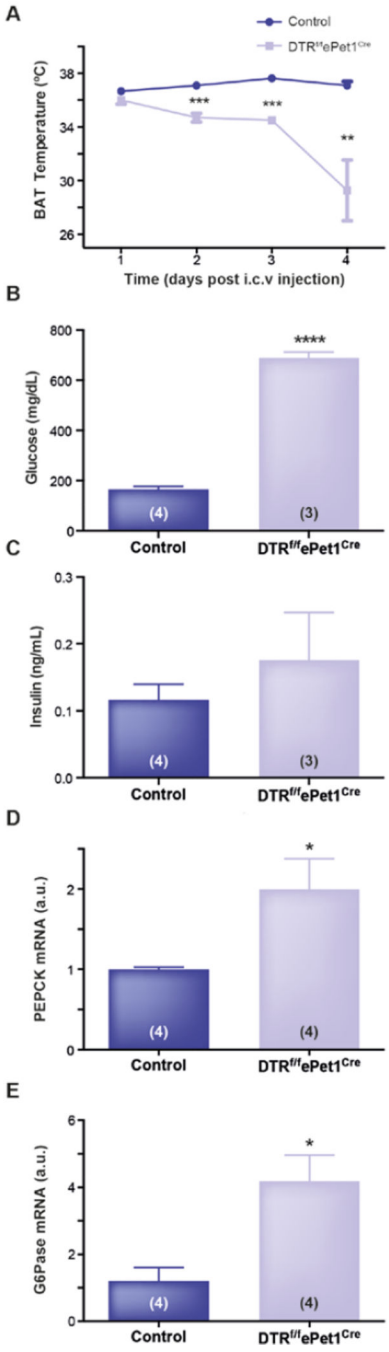

Figure 4. Ablation of Pet-1+ Neurons with Intracerebroventricular Injection of DT Decreases BAT Temperature, Causes Hyperglycemia, and Increases Hepatic Gluconeogenic Gene Expression without Changing Systemic Insulin Levels

(A–E) BAT temperature (A), plasma glucose (B), insulin (C), PEPCK mRNA expression (D), and G6Pase mRNA expression (E) in controls and i.c.v. DT-treated *DTR$^{f/f}$ePet1^{Cre}* mice. Data are presented as mean ± SEM. *p < 0.05, **p < 0.01, ***p < 0.005, ****p < 0.001.

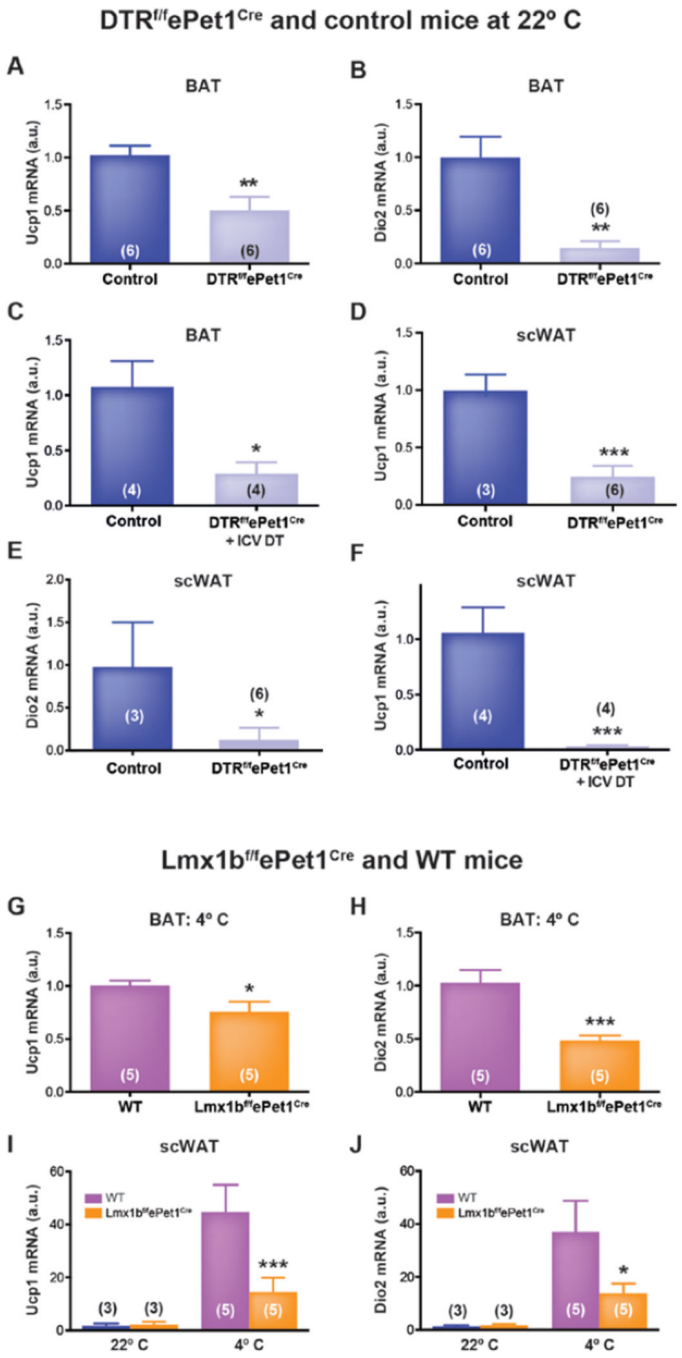

Figure 5. Acute, developmental, and i.c.v. ablation of central *Pet-1*+ neurons reduces thermogenic gene expression in brown and beige fat

(A and B) Ucp1 (A) and Dio2 (B) expression in interscapular BAT of i.p. DT-treated DTRf/fePet1Cre mice and controls.

(C) Ucp1 expression in interscapular BAT of i.c.v. DT-treated *DTR$^{f/f}$ePet1^{Cre}* mice and controls.

(D and E) Expression of Ucp1 (D) and Dio2 (E) transcripts in inguinal scWAT of i.p. DT-treated *DTR$^{f/f}$ePet1^{Cre}* mice and controls.

(F) Ucp1 expression in inguinal scWAT of i.c.v. DT-treated *DTR*$^{f/f}$*ePet1*^{Cre} mice and controls.

(G and H) Ucp1 (G) and Dio2 (H) expression in interscapular BAT of cold-exposed *Lmx1b*$^{f/f}$*ePet1*^{Cre} mice and controls.

(I and J) Cold-evoked induction of Ucp1 (I) and Dio2 (J) transcription in inguinal scWAT of *Lmx1b*$^{f/f}$*ePet1*^{Cre} mice. Data presented as mean ± SEM. *p < 0.05, **p < 0.01, ***p < 0.005.

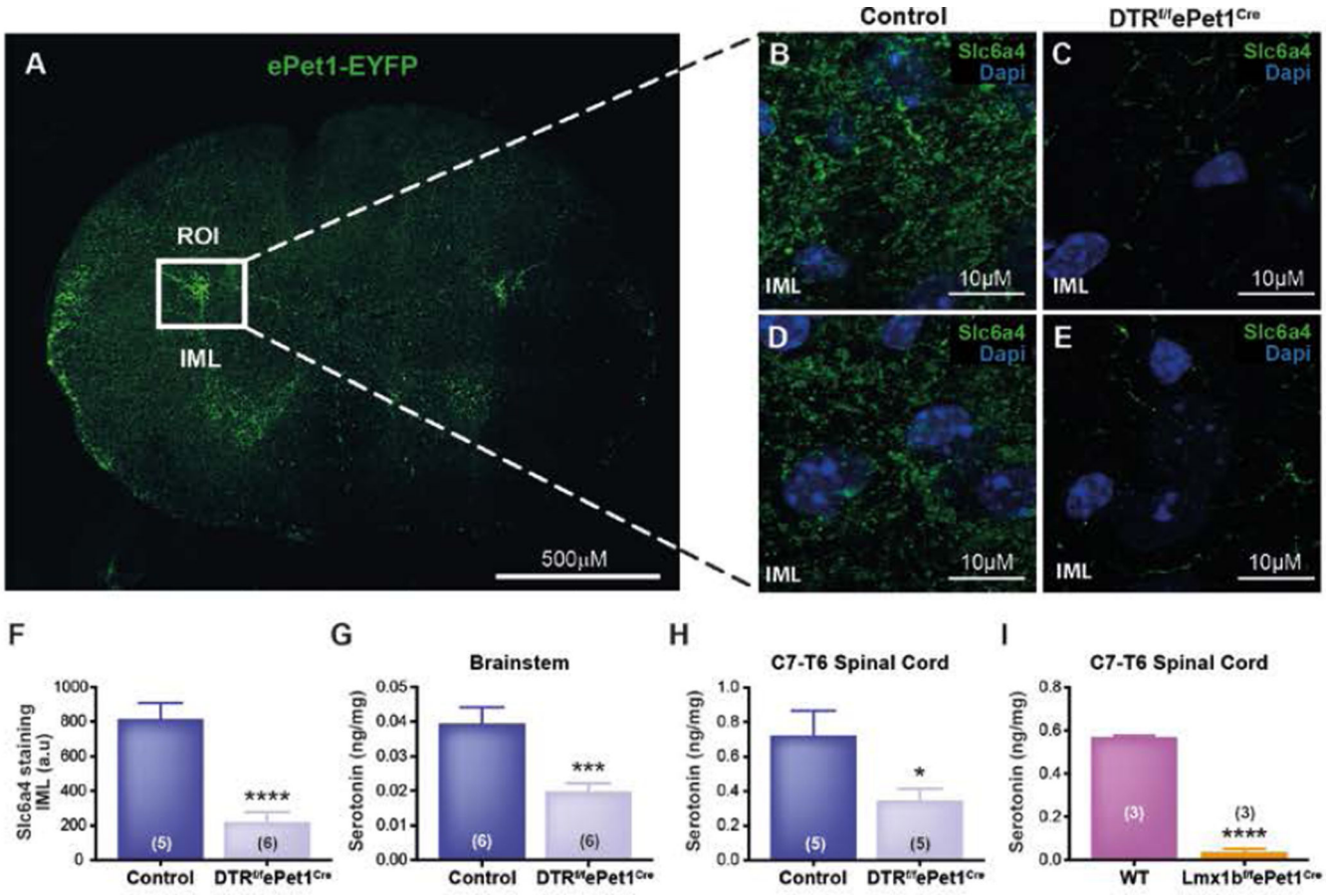

Figure 6. Pet-1+ Neurons of the Ventromedial Medulla Primarily Project to the Intermediolateral Cell Column in the Spinal Cord, and These Projections Are Lost in Lmx1bf/fePet1Cre Mice and DT-Treated DTRf/fePet1Cre Mice

(A) EYFP expression in the thoracic spinal cord (T2–T5) of ePet1-EYFP mice, with the intermediolateral cell column indicated by a box.

(B) Serotonin transporter (Slc6a4) expression in control upper thoracic spinal cord IML.

(C) Serotonin transporter (Slc6a4) expression in i.p. DT-treated thoracic spinal cord IML.

(D) An additional control animal upper thoracic spinal cord IML, stained for serotonin transporter (Slc6a4).

(E) An additional i.p. DT-treated thoracic spinal cord IML, stained for serotonin transporter (Slc6a4).

(F) Quantification of the serotonin transporter density within the spinal cord IML.

(G and H) 5-HT levels in the raphe´ (G) and thoracic spinal cord (H) of control and i.p.

(I) DT-treated $DTR^{f/f}ePet1^{Cre}$ mice 5-HT levels in the thoracic spinal cord of $Lmx1b^{f/f}ePet1^{Cre}$ mice.

Data are presented as mean ± SEM. *p < 0.05, **p < 0.01, ***p < 0.005, ****p < 0.001.